Narrowband to broadband conversions of land surface albedo: II. Validation

Shunlin Liang [a,*], Chad J. Shuey [a], Andrew L. Russ [b], Hongliang Fang [a], Mingzhen Chen [a], Charles L. Walthall [b], Craig S.T. Daughtry [b], Raymond Hunt Jr. [b]

[a]Laboratory for Global Remote Sensing Studies, 2181 LeFrak Hall, Department of Geography, University of Maryland, College Park, MD 20742, USA
[b]Hydrology and Remote Sensing Laboratory, USDA ARS, Beltsville, MD 20705, USA

Abstract

In the first paper of this series, we developed narrowband to broadband albedo conversion formulae for a series of sensors. These formulae were determined based on extensive radiative transfer simulations under different surface and atmospheric conditions. However, it is important to validate the simulation results using independent measurement data. In this paper, the validation results for three broadband albedos (total-shortwave, -visible and -near-IR albedos) using ground measurement of several cover types on five different days at Beltsville, MD are presented. Results show that the conversion formulae in the previous paper are very accurate and the average residual standard errors of the resulting broadband albedos for most sensors are around 0.02, which meets the required accuracy for land surface modeling.
© 2002 Published by Elsevier Science Inc.

1. Introduction

It has been well recognized that surface albedo is among the main radiative uncertainties in current climate modeling. Remote sensing is the only practical means for mapping land surface albedo globally. Broadband albedo is usually estimated from broadband sensors, but the accurate determination of land surface broadband albedo from top-of-atmosphere (TOA) observations requires the knowledge of atmospheric conditions and surface characteristics, which can be monitored effectively only by multispectral sensors. Narrowband multispectral observations also have much finer spatial resolutions that allow us to characterize both the surface and atmospheric heterogeneity (Liang, Stroeve, Grant, Strahler, & Duvel, 2000).

The derivation of surface broadband albedos from narrowband observations requires several levels of processing, including (1) atmospheric correction that converts TOA radiance to surface directional reflectance, (2) surface angular modeling that converts surface directional reflectance to spectral albedo, and (3) narrowband to broadband albedo conversions. We mainly deal with the last process in this paper. Many studies on converting narrowband to broadband albedos reported in the literature were based on either field measurements of certain surface types or model simulations that incorporated a very limited number of surface reflectance spectra. Therefore, their formulae have limited applications. Moreover, the conversion formulae were mostly for total shortwave broadband albedo. In the first paper of this series (Liang, 2001), we established a series of conversion formulae based on extensive radiative transfer simulations. A new method was developed to decouple surface reflectance spectra from the radiative transfer simulations so that many different surface reflectance spectra and atmospheric conditions can be effectively incorporated. The formulae for converting to seven broadband albedos were provided for several narrowband sensors, including Advanced Spaceborne Thermal Emission and Reflection Radiometer (ASTER), Advanced Very High Resolution Radiometer (AVHRR), Geostationary Operational Environmental Satellite (GOES), LANDSAT 7 Enhanced Thematic Mapper Plus (ETM+), Multiangle Imaging SpectroRadiometer (MISR), Moderate Resolution Imaging Spectroradiometer (MODIS), Polarization and Directionality of Earth's Reflectances (POLDER), and VEGETATION on the SPOT spacecraft. These seven broadband albedos include total shortwave, total-, direct- and diffuse-visible albedos, and total-, direct- and diffuse-near-IR

---

* Corresponding author. Tel.: +1-301-405-4556; fax: +1-301-314-9299.
E-mail address: sliang@geog.umd.edu (S. Liang).

albedos that are needed by many land surface models. Although some of these formulae were compared with the published formulae of the same sensors in the first paper, these formulae need to be validated comprehensively before used for various applications.

In this study, extensive ground measurements have been conducted to validate these formulae. Ideally, spectral albedos and broadband albedos should be measured simultaneously. But we could not find any existing instruments for measuring spectral albedo directly. On the other hand, the nadir-viewing reflectances are highly correlated with spectral albedos if the surface does not have dominating three-dimensional structures (e.g., trees) and the solar zenith angle is not very large. If the surface can be assumed to be Lambertian, surface reflectance numerically equals spectral albedo. Therefore, spectral reflectance and broadband albedos were measured simultaneously over different cover types at different solar zenith angles for the purpose of validation.

In the following, we will start with a brief summary of the data simulation and results from the previous paper (Liang, 2001). The validation sites and experiment designs are then described. The surface cover types and the description of the general conditions are also provided. Data analysis and validation results are presented in Section 5. A brief conclusion is given at the end.

2. Brief summary of the conversion formulae

The earlier studies on converting narrowband to broadband albedos in the literature were based on either field measurements of certain surface types or model simulations under limited conditions. It is impossible to develop a universal formula based only on ground measurements because it is so expensive to collect extensive "ground truths" under different atmospheric and surface conditions. Simulation studies reported in the literature usually use a very limited number of surface reflectance spectra since incorporating many different surface reflectance spectra into the radiative transfer simulations is very computationally expensive. As a result, there are many different conversion formulae for the same sensor resulting from different methods and data sets. There is a pressing need to develop general conversion formulae for universal application. In our previous paper (Liang, 2001), a novel approach is developed so that hundreds of measured reflectance spectra of different cover types are incorporated into the simulation results without introducing too much computational burden.

Conversion formulae in the literature are mainly for total shortwave albedo in the calculation of surface radiation budget. However, many land surface models (e.g., Kiehl et al., 1996; Koster & Suarez, 1992; Sellers et al., 1996) have divided the total shortwave into visible and near-IR broadbands, and visible and near-IR albedos are further divided

into direct and diffuse components. Thus, we generated seven broadband albedos (total shortwave, total visible, direct and diffuse visible, total near-IR, direct and diffuse near-IR) from the extensive simulation. The simulated surface spectral albedos were then integrated with the different sensor spectral response functions to form the narrowband albedos.

For ease of reference, the conversion formulae for the total shortwave, visible and near-IR albedos are given below. In all cases, α_i on the right side of the equations represents spectral albedos. The spectral bands of these narrowband sensors are specified in Table 1. Note that some constant terms are too small and have been dropped.

For the total shortwave broadband albedo,

$$\alpha^{\text{ASTER}} = 0.484\alpha_1 + 0.335\alpha_3 - 0.324\alpha_5 + 0.551\alpha_6 \\ + 0.305\alpha_8 - 0.367\alpha_9 - 0.0015$$

$$\alpha^{\text{AVHRR}} = -0.3376\alpha_1^2 - 0.2707\alpha_2^2 + 0.7074\alpha_1\alpha_2 \\ + 0.2915\alpha_1 + 0.5256\alpha_2 + 0.0035$$

$$\alpha^{\text{GOES}} = 0.0759 + 0.7712\alpha$$

$$\alpha^{\text{ETM+}} = 0.356\alpha_1 + 0.130\alpha_3 + 0.373\alpha_4 \\ + 0.085\alpha_5 + 0.072\alpha_7 - 0.0018$$

$$\alpha^{\text{MISR}} = 0.126\alpha_2 + 0.343\alpha_3 + 0.415\alpha_4 + 0.0037$$

$$\alpha^{\text{MODIS}} = 0.160\alpha_1 + 0.291\alpha_2 + 0.243\alpha_3 + 0.116\alpha_4 \\ + 0.112\alpha_5 + 0.081\alpha_7 - 0.0015$$

$$\alpha^{\text{POLDER}} = 0.112\alpha_1 + 0.388\alpha_2 - 0.266\alpha_3 \\ + 0.668\alpha_4 + 0.0019$$

$$\alpha^{\text{VEGETATION}} = 0.3512\alpha_1 + 0.1629\alpha_2 \\ + 0.3415\alpha_3 + 0.1651\alpha_4 \qquad (1)$$

For total visible albedo,

$$\alpha^{\text{ASTER}} = 0.820\alpha_1 + 0.183\alpha_2 - 0.034\alpha_3 \\ - 0.085\alpha_4 - 0.298\alpha_5 + 0.352\alpha_6 \\ + 0.239\alpha_7 - 0.240\alpha_9 - 0.001$$

$$\alpha^{\text{AVHRR}} = 0.5975\alpha_1 + 0.4410\alpha_1^2 + 0.0074$$

$$\alpha^{\text{GOES}} = 0.689\alpha + 0.3604\alpha^2 - 0.0084$$

$$\alpha^{\text{ETM+}} = 0.443\alpha_1 + 0.317\alpha_2 + 0.240\alpha_3$$

$$\alpha^{\text{MISR}} = 0.381\alpha_1 + 0.334\alpha_2 + 0.287\alpha_3$$

$$\alpha^{\text{MODIS}} = 0.331\alpha_1 + 0.424\alpha_3 + 0.246\alpha_4$$

$$\alpha^{\text{POLDER}} = 0.533\alpha_1 + 0.412\alpha_2 + 0.215\alpha_3 \\ - 0.168\alpha_4 + 0.0046$$

$$\alpha^{\text{VEGETATION}} = 0.5717\alpha_1 + 0.4277\alpha_2 + 0.0033 \qquad (2)$$

Table 1
Spectral bands of the narrowband sensors

Sensors	Spectral bands and their wavelength ranges (µm)								
	1	2	3	4	5	6	7	8	9
ASTER	0.52−0.6	0.63−0.69	0.78−0.86	1.6−1.7	2.15−2.18	2.18−2.22	2.23−2.28	2.29−2.36	2.36−2.43
AVHRR-14	0.57−0.71	0.72−1.01	–	–	–	–	–	–	–
GOES-8	0.52−0.72	–	–	–	–	–	–	–	–
ETM+	0.45−0.51	0.52−0.6	0.63−0.69	0.75−0.9	1.55−1.75	–	2.09−2.35	–	–
MISR	0.42−0.45	0.54−0.55	0.66−0.67	0.85−0.87	–	–	–	–	–
MODIS	0.62−0.67	0.84−0.87	0.46−0.48	0.54−0.56	1.23−1.25	1.63−1.65	2.11−2.15	–	–
POLDER	0.43−0.46	0.66−0.68	0.74−0.79	0.84−0.88	–	–	–	–	–
VEGETATION	0.43−0.47	0.61−0.68	0.78−0.89	1.58−1.75	–	–	–	–	–

For total near-IR broadband albedos,

$$\alpha^{ASTER} = 0.654\alpha_3 + 0.262\alpha_4 - 0.391\alpha_5 + 0.500\alpha_6 - 0.002$$

$$\alpha^{AVHRR} = -1.4759\alpha_1^2 - 0.6536\alpha_2^2 + 1.8591\alpha_1\alpha_2 + 1.063\alpha_2$$

$$\alpha^{ETM+} = 0.693\alpha_4 + 0.212\alpha_5 + 0.116\alpha_7 - 0.003$$

$$\alpha^{MISR} = -0.387\alpha_1 - 0.196\alpha_2 + 0.504\alpha_3 + 0.830\alpha_4 + 0.011$$

$$\alpha^{MODIS} = 0.039\alpha_1 + 0.504\alpha_2 - 0.071\alpha_3 + 0.105\alpha_4$$
$$+ 0.252\alpha_5 + 0.069\alpha_6 + 0.101\alpha_7$$

$$\alpha^{POLDER} = -0.397\alpha_1 + 0.451\alpha_2 - 0.756\alpha_3$$
$$+ 1.498\alpha_4 + 0.0013$$

$$\alpha^{VEGETATION} = 0.6799\alpha_3 + 0.3157\alpha_4 - 0.0038 \qquad (3)$$

Linear and nonlinear regression analyses are then applied to generate the conversion formulae. It is interesting to note that most conversion formulae are linear. Although paper I compared some of these formulae with previously published formulae, a comprehensive validation is still needed. This paper describes field observations that go some way towards the validation.

3. Validation site and experimental design

All field measurements were taken in the validation site located at northeast of Washington DC covering NASA/ GSFC (Goddard Space Flight Center) and USDA (US Department of Agriculture) BARC (Beltsville Agricultural Research Center). This is an area of diverse soils, crops, and natural vegetation cover. At this site we are concurrently validating a series of satellite products, including the NASA MODIS and MISR BRDF (Bidirectional Reflectance Distribution Function) and albedo products, and the NASA EO-1 (Earth Observer-1) products. Several other projects (e.g., USDA/BARC precision farming and canopy biochemistry, high-resolution IKONOS data validation project through the NASA science data buy program) are also conducting field experiments jointly at this site. This site has been identified as one of 24 NASA EOS (Earth Observing System) Land

Core Validation Sites (Justice, Starr, Wickland, Privette, & Suttles, 1998; Morisette et al., 1999).

From May 2000 to March 2001, two albedometers (one for total shortwave albedo and another for total near-IR albedo) and the ASD (Field Spec Pro, Analytical Spectral Devices) hand-held spectroradiometer were used in our validation site to measure surface reflectance spectra and broadband albedos simultaneously over different cover types.

Two measurement approaches were used in our validation experiments. The first approach measured albedo over multiple cover types. On May 11 and August 2, 2000, different cover types were measured by moving these instruments from one site to another. The second approach aims at albedo measurements of diurnal cycles of typical cover types in our test site. On February 26, March 1 and March 28, 2001, we measured the diurnal cycles of broadband albedos with one minute sampling by fixing albedometers over three cover types: green crop (February 26),

Table 2
Measurement times and atmospheric conditions

Cover type	Time	SZA	AOD (440 nm)	Water vapor
May 11, 2000				
Wheat field	11:17–11:40 am	31.46	0.18	0.96
Vetch	11:43–11:51 am	27.81	0.19	0.99
Corn stubble	12:34–12:46 pm	21.64	0.19	1.1
Live hairy vetch	12:54–1:04 pm	21.03	0.18	1.32
Soil	3:19–3:26 pm	36.69	0.17	1.37
Grass	3:30–3:36 pm	38.47	0.17	1.37
Dead vetch	4:12–4:22 pm	46.62	0.17	1.54
August 4, 2000				
Grass 1	9:45–9:56 am	49.2	1.03	4.63
Soybean 1	10:01–10:12 am	46.18	1.03	4.63
Weed 1	10:17–10:29 am	43.01	1.03	4.63
Soybean 2	10:33–10:43 am	40.28	1.03	4.63
Soybean 3	11:15–11:26 am	33.05	1.03	4.63
Weed 2	11:30–11:40 am	30.7	1.03	4.63
Dry soil	12:13–12:25 pm	25.07	1.03	4.63
Low dense grass	12:28–12:40 pm	23.51	0.99	4.67
Medium sparse grass	12:59–1:09 pm	22.03	0.87	4.73
Soil 2	1:18–1:28 pm	22.05	0.68	4.7
Tall grass	2:39–2:49 pm	29.49	3.81	4.91

dry yellow grass (March 1) and black asphalt (March 28). The ASD was used to measure surface spectral reflectance about every one hour.

Each albedometer consists of two CM21 pyranometers with one pointing up and another down. Near-IR albedometers are the same as the shortwave albedometers with filters added by the manufacturer (Kipp and Zonen). The factory calibration has been used. Two albedometers allow us to measure three broadband albedos: total shortwave, total visible and total near-IR. Note that the total visible albedo is actually calculated from the measured total shortwave fluxes and total near-IR fluxes. Although we cannot validate direct and diffuse visible and near-IR broadband albedos, if these three total broadband albedos are well predicted by the conversion formulae the same conclusion can be drawn for other four broadband albedos since all data came from the same database generated from the same radiative transfer software package in our earlier study (Liang, 2001).

The ASD spectroradiometer is a commercial product that measures upwelling radiance. The ratio of the upwelling radiance of the target to that of a standard white reference panel generates the spectral reflectance with a very high spectral resolution (1 nm). Since the nadir reflectance is highly related to spectral albedo, we measured reflectance at nadir only. These spectra were then integrated to narrowband reflectances using the sensor spectral response functions.

The albedometers were fixed at the two ends of a horizontal pole, supported about 1.5 m above ground. The ASD spectroradiometer has a very small ground sampling size of about 0.75 m. Most surfaces are quite heterogeneous at that scale. However, the albedometers measure an average albedo of a much larger region because of the multiple interactions between atmosphere and surface. To match both, multiple samples were measured by using the ASD radiometer over each cover type.
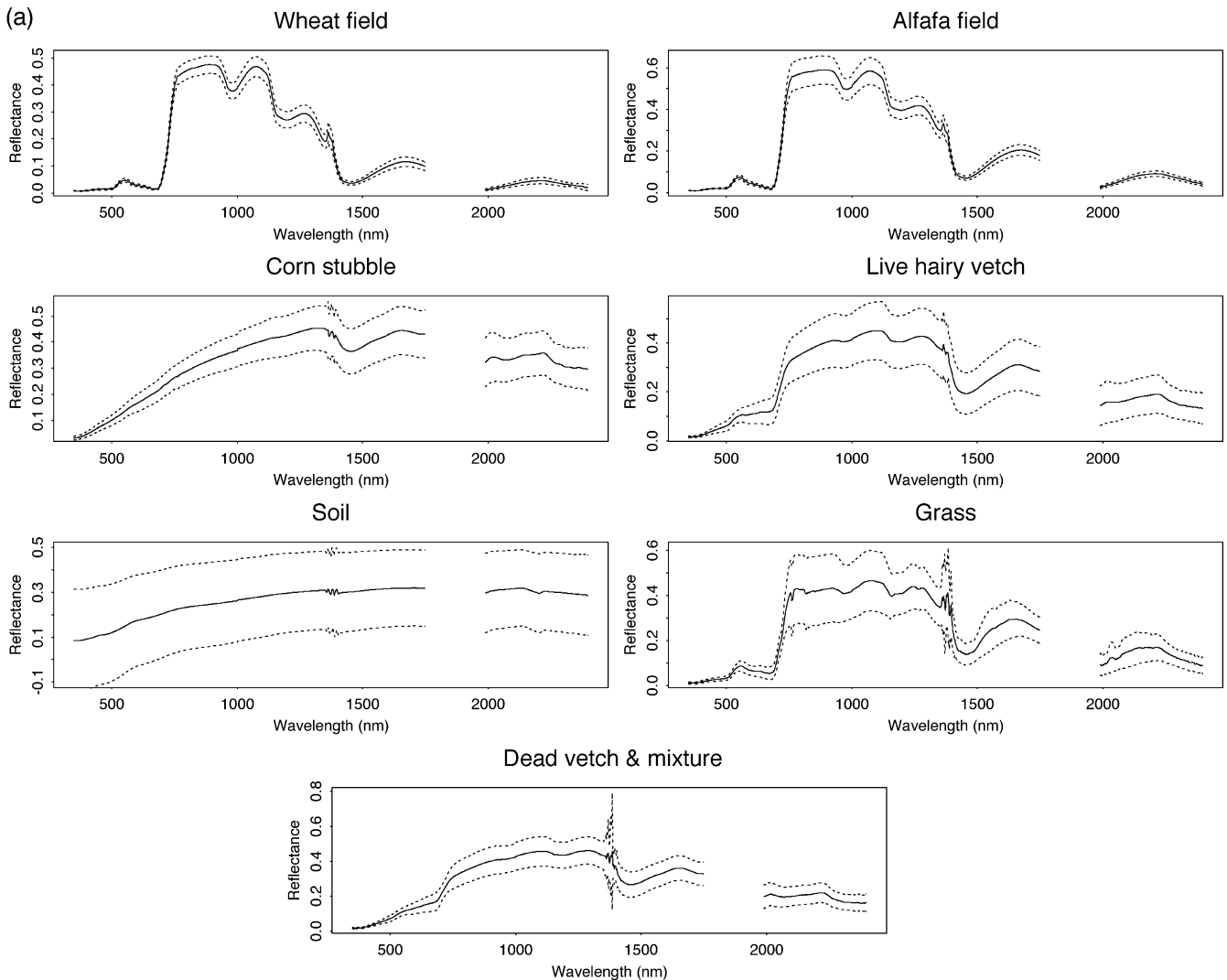

Fig. 1. Average (solid line) reflectance spectra and plus/minus one standard deviation (dashed line) for different cover types measured on May 11 and August 4, 2000.
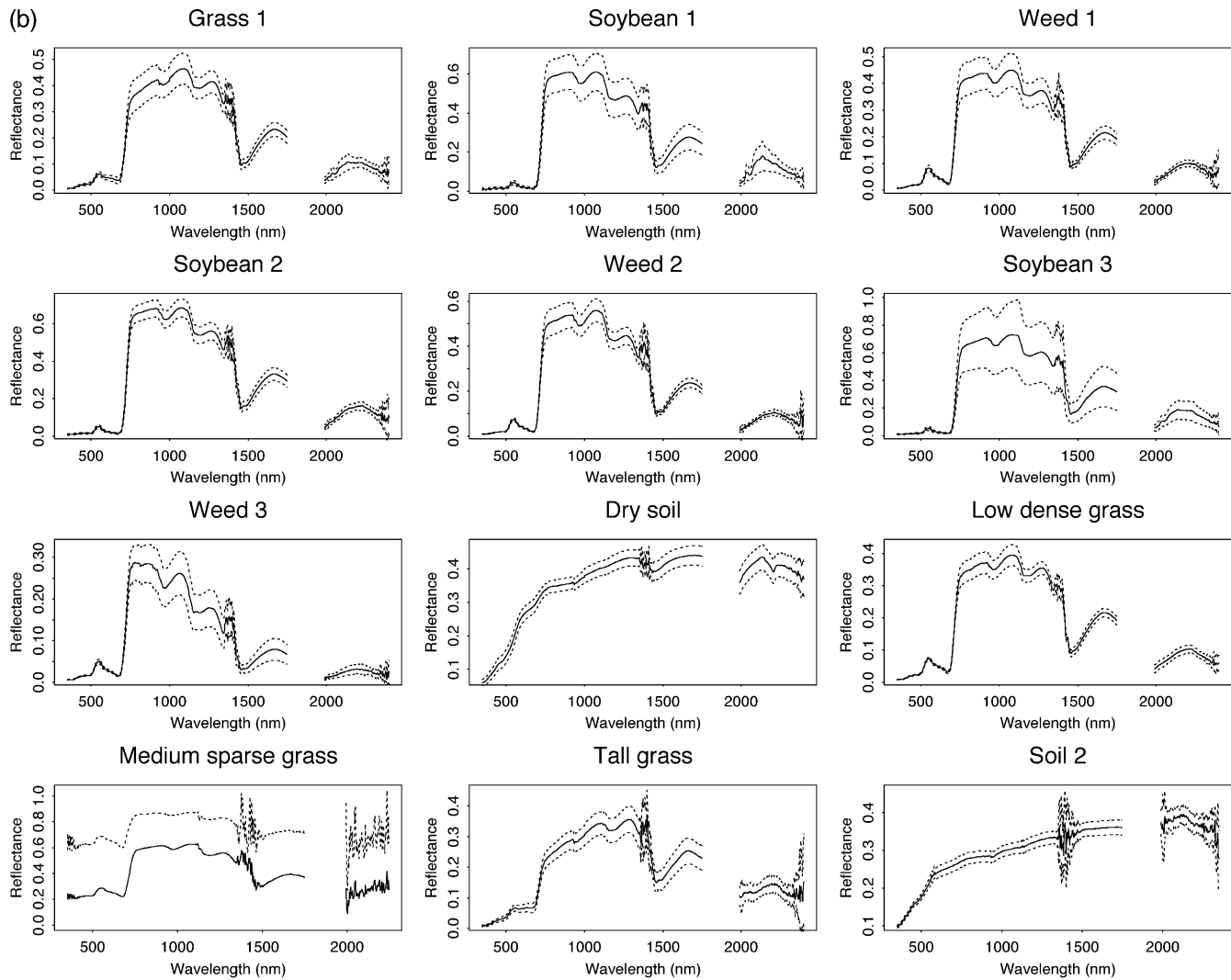
(b)

Fig. 1 (*continued*).

On the 5 days that samples were taken, the atmospheric conditions were different. For demonstration purposes, the land surface cover type, measurement time, solar zenith angle and the aerosol optical depth and water vapor on both May 11 and August 4 are listed in Table 2. Aerosol optical depth and total water vapor content were measured by a Sunphotometer located in NASA/GSFC, part of our validation site. Our measurements times are matched with the closest aerosol optical depth and total water vapor content readings available.

4. Cover types and conditions

4.1. Albedo measurements of multiple cover types

On both May 11 and August 4, 2000, broadband albedos and reflectance spectra for a series of land covers were measured. A brief description of these cover types and atmospheric conditions follows.

4.1.1. May 11, 2000

May 11, 2000 was a clear, relatively cool day and with the exception of a few scattered clouds there were clear atmospheric conditions. In general vegetation and crops were in typical early Spring growing season form. Seven cover types were measured.

The first site was a wheat field, with mature pre-harvest winter wheat which was green in color and very dense. The second site is a field of hairy vetch and alfalfa with a small proportion of weed and exposed soil. The spectrum is also typical of green vegetation. Next was a recently planted cornfield consisting mainly of exposed soil, but also yellow-brown corn stubble from the previous year's harvest, and tiny green sprouts of corn from the current season's planting. These sprouts
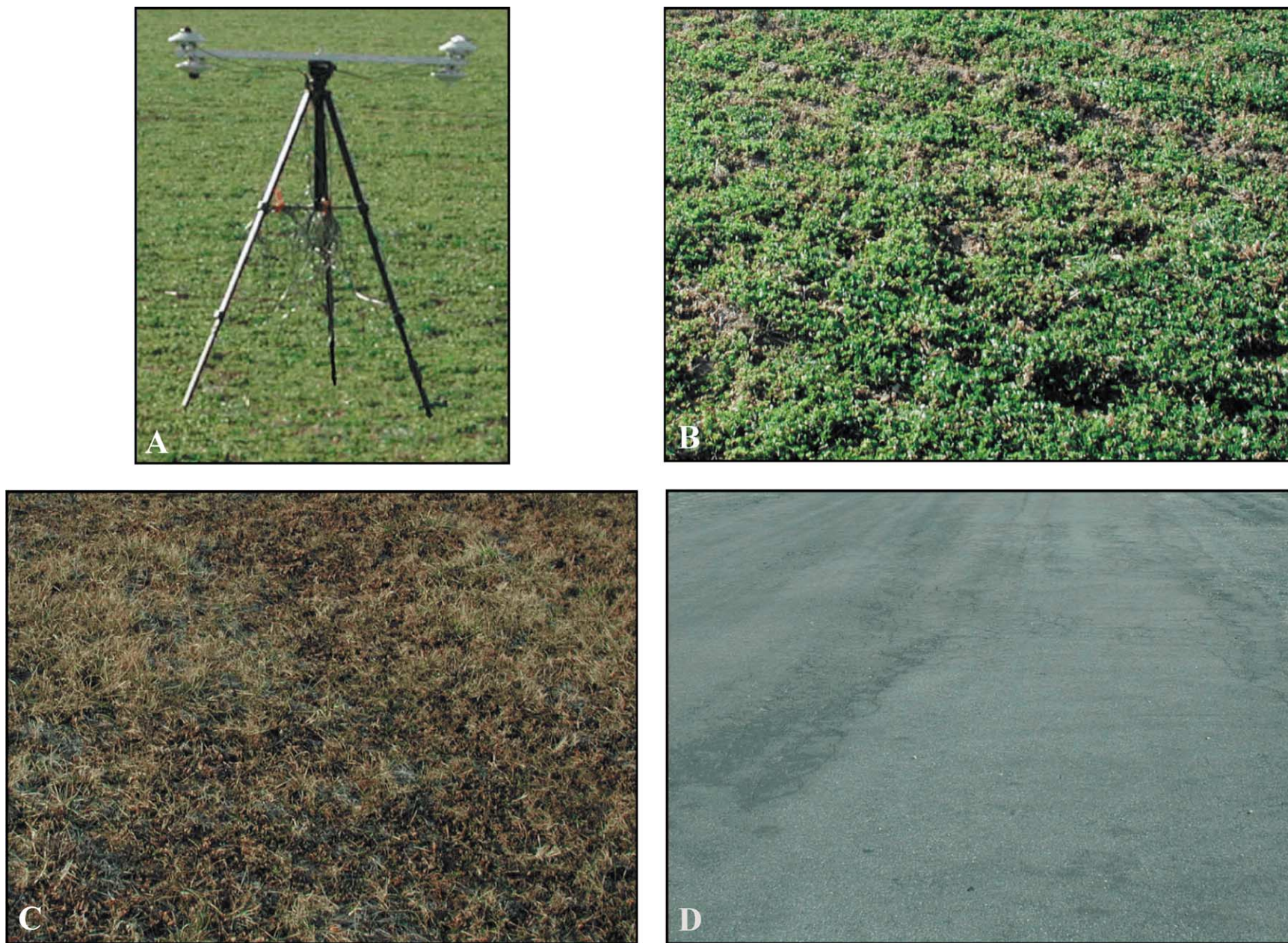
Fig. 2. Three cover types for which the diurnal cycle of the broadband albedo was measured.
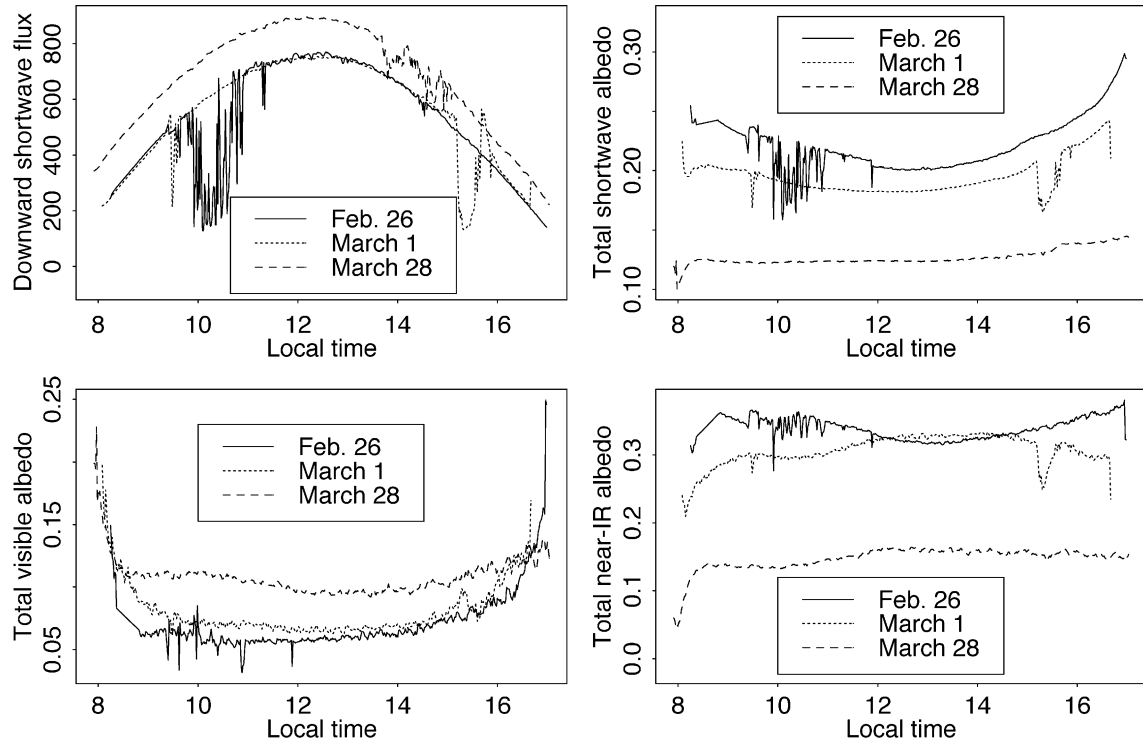
Fig. 3. The measured diurnal cycles of the broadband albedos.

were only 2–3 in. tall. The next site is hairy vetch, which also showed a typical vegetation spectrum. The next site was recently plowed soil, followed by orchard grass. Finally, the last site was a mixture of dead hairy vetch, weed and grasses, which was distinctly yellow in color. It had been treated with herbicide in the previous weeks to kill the vetch and prepare the field for a mid-season planting. Its spectrum largely resembles bare soil, but a trace of vegetation response is detectable.

4.1.2. August 4, 2000

August 4, 2000 was a mild summer day in the middle-late growing season with moderately humid and hazy atmospheric conditions. The recent weather had been relatively cool and dry. Twelve cover types were measured.

Four different grass covers were measured. These included one area of sparse grass where dry soil was largely visible from above and grass height was 0.5–1 m.
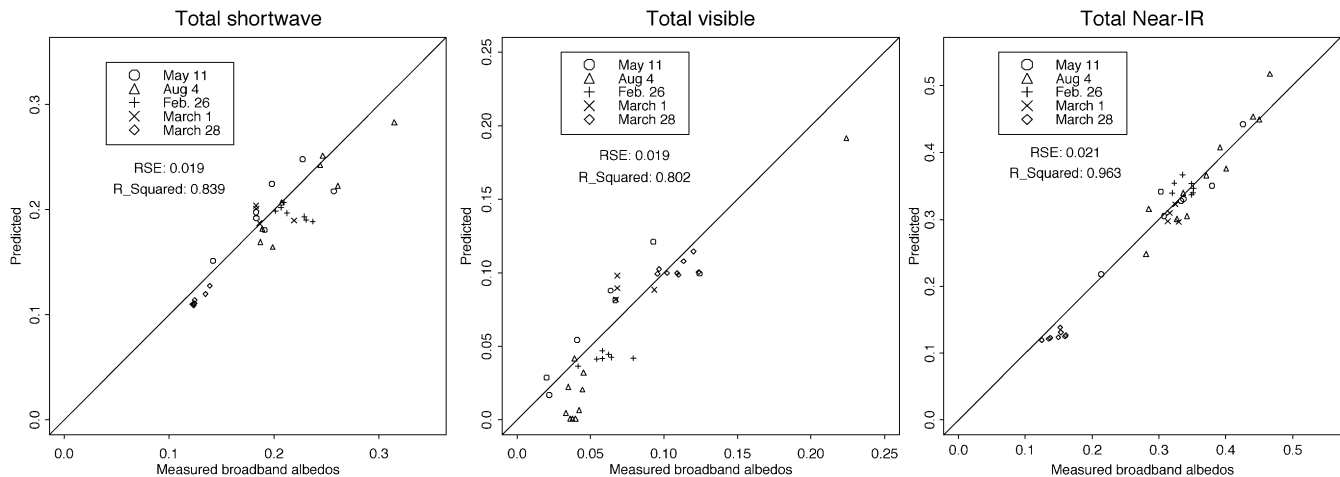

Fig. 4. Comparison of the measured and predicted three broadband albedos from ASTER.
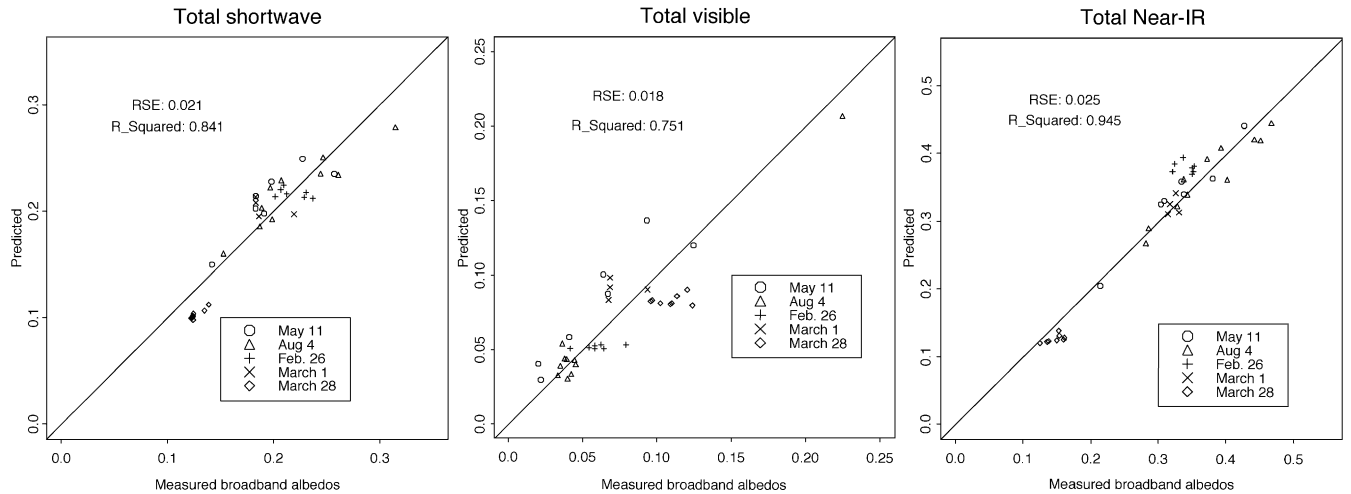
Fig. 5. Comparison of the measured and predicted three broadband albedos from AVHRR.

The second area was dense, dark green grass about 10 cm in height but with almost no visible soil. The next was taller grass around a meter in height and of moderate density, though little background was visible. Finally, the last grass cover area was a very tall grass over a meter in height with moderate density. Of the four grass types, only the second appeared to have had any significant management over the past years, the other three had
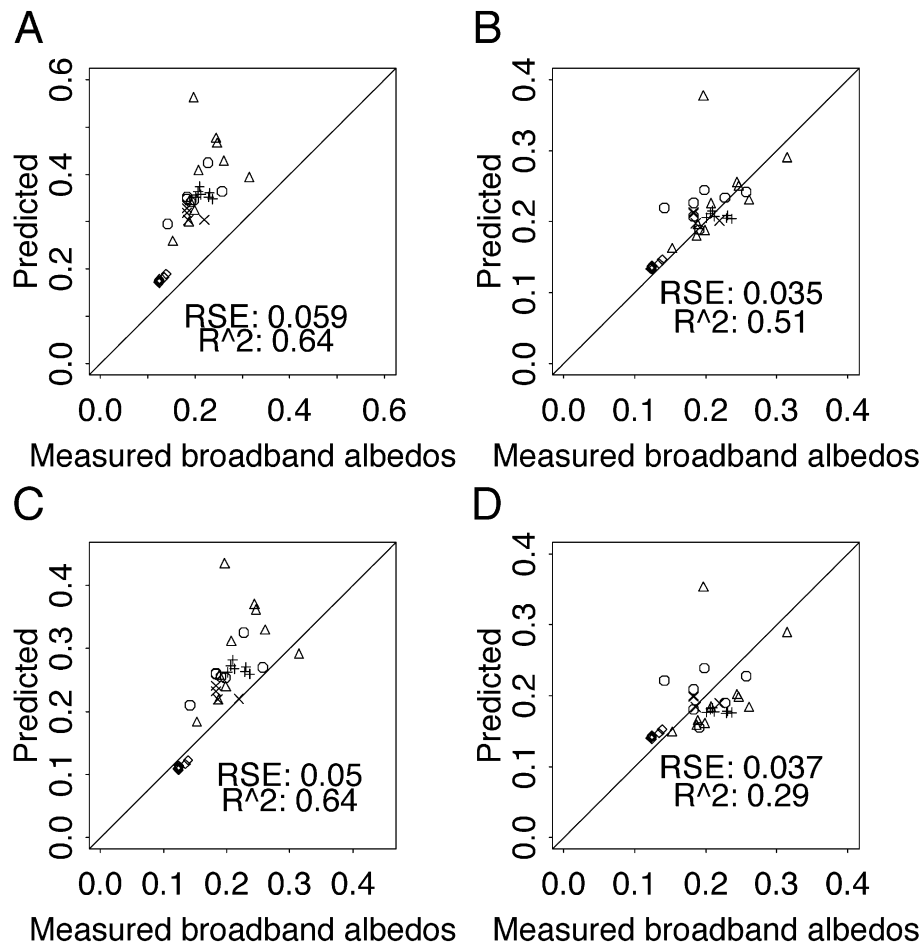
Fig. 6. Comparison of the measured shortwave albedos with these predicted from Russell, Nunez, Chladil, Valiente, and Lopez-Baeza (1997) (A), Valiente, Nunez, Lopez-Baeza, and Moreno (1995) (B), Key (1996) (C) and Stroeve, Nolin, and Steffen (1997) (D) for the AVHRR sensor. The symbols are the same as those in the previous figure.
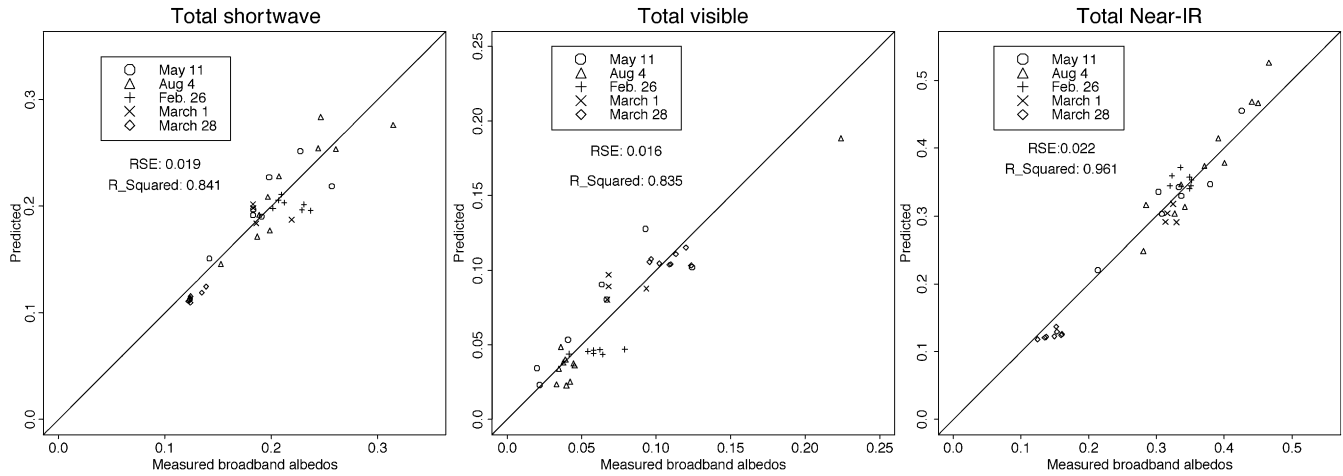
Fig. 7. Comparison of the measured and predicted three broadband albedos from ETM+/TM.

grown wild in an abandoned airport area. All grass areas showed similar spectra, typical of green vegetation, with reflectances peaking at 0.4 around 1100 nm, except for the sparse grass with higher reflectances due to the exposed soil. Three areas of soybean were also measured. The first two show considerable spectral similarities, the third had a higher reflectance. Three weed areas were also measured, each with differing densities and heights. Finally, two areas of bare soil were measured. The first was very dry, and light brown in color, the second was dry, very gravelly and also light in color. Both spectra were typical of dry soil.
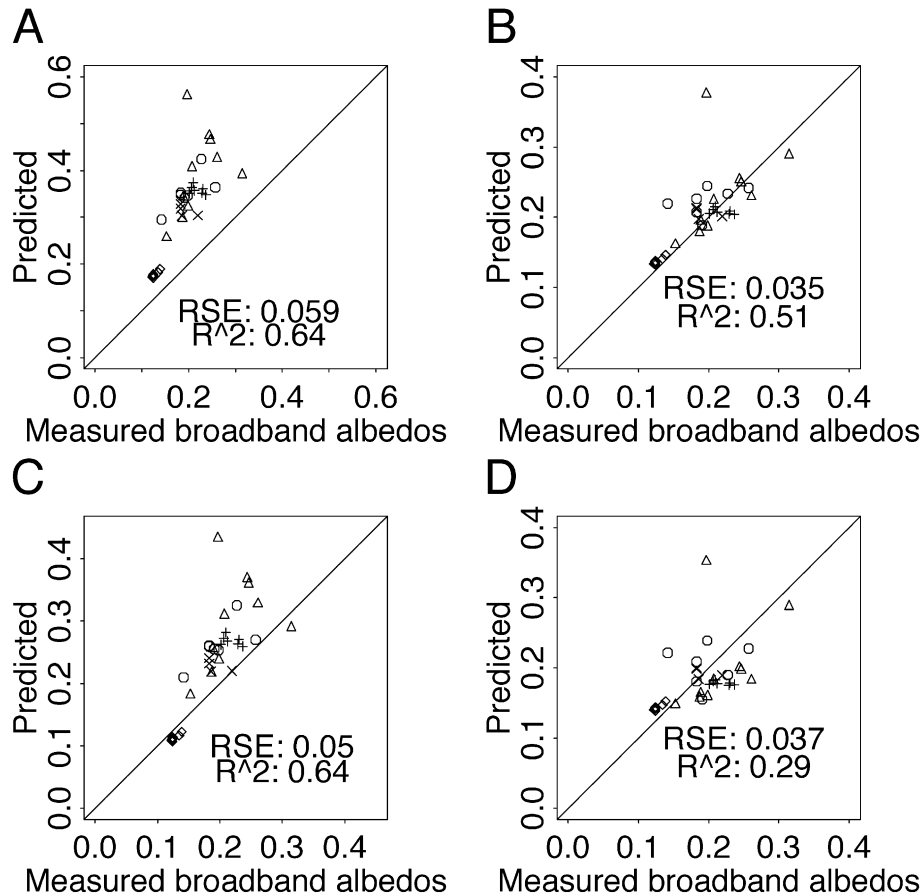

Fig. 8. Comparison of the measured shortwave albedos with the predicted from Brest and Goward (1987) (A) and Duguay and LeDrew (1992) (B) for the TM sensor. The symbols are the same as those in the previous figure.

(a)

Band4 TOA reflectance
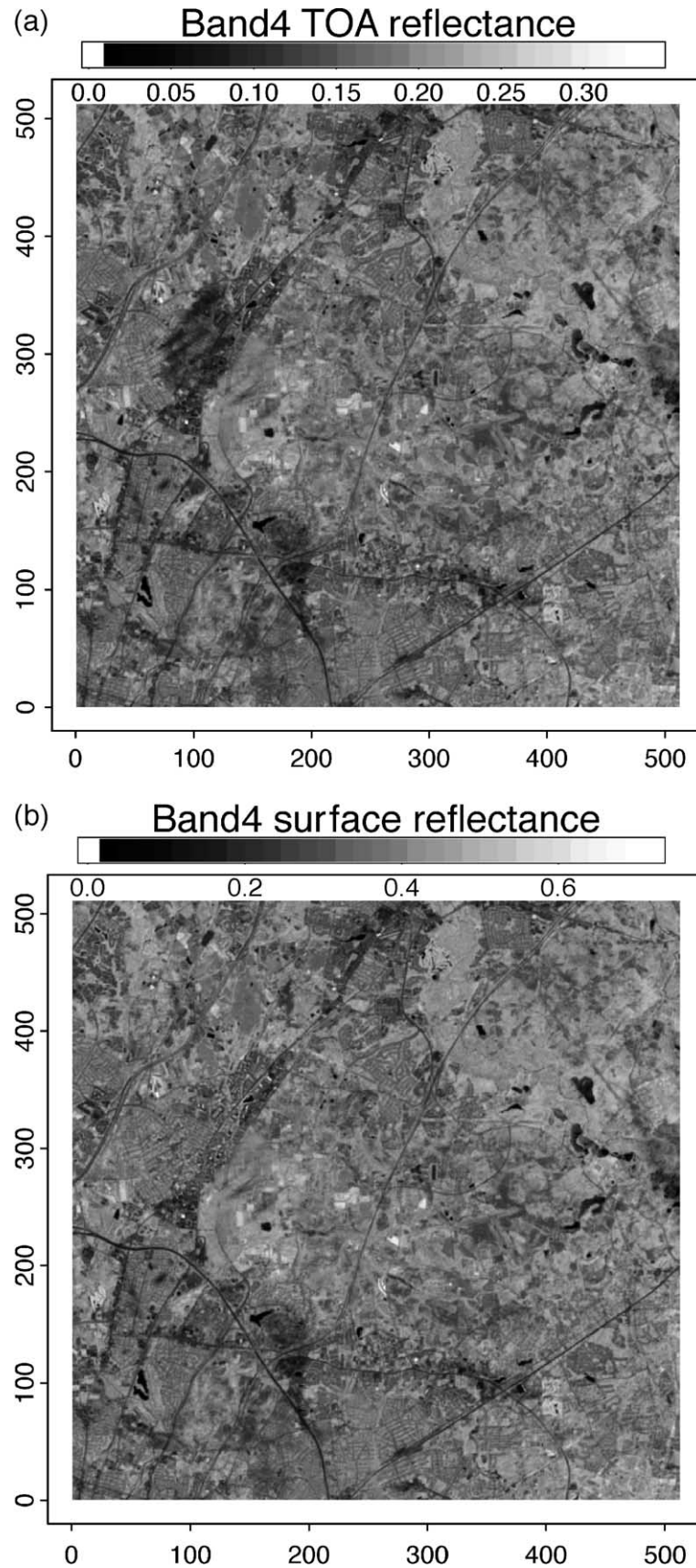

(b)

Band4 surface reflectance

Fig. 9. Landsat-7 ETM+ band 4 images of May 11, 2000 over the USDA BARC validation site at Beltsville, MD before (A) and after (B) atmospheric correction. The major visual difference between these two images is the removal of shadows in the corrected imagery.

On May 11 and August 4, 2000, the albedometers were used to measure over each cover type for 10–15 min with 1-min sampling intervals. Because of the variations of the atmospheric conditions, temporally averaged broadband albedos were then calculated for each cover type. ASD measurements took place simultaneously during this period of time. There are 50–100 reflectance spectra measured by the ASD radiometer for each cover type. Because of the surface heterogeneity, an average was also calculated to represent the condition of each cover type. The average reflectance spectrum is then integrated with sensor spectral response functions to get narrowband reflectance. The mean reflectance spectra for each cover type at two dates (May 11 and August 4) are shown in Fig. 1. The dashed lines denote one standard deviation. From this figure, we can see that most cover types have quite variable reflectances spatially, but medium sparse grass measured on August 4 was quite mixed and their standard deviation is very large. This is also true for the soil measured on May 11 due to roughness, moisture condition, and other factors.

It is important to note that the measured surface reflectance spectra were not used in the simulation study that led to these conversion formulae presented in the first paper of the series. The measured spectra form an independent data set for this validation.

4.2. Diurnal cycle measurements

Surface radiation budget studies must consider all local times through the diurnal cycle. Both modeling and measurements (Dickinson, 1983; Grant, Prata, & Cechet, 2000; Kimes, Sellers, & Newcomb, 1987; Pinker, Thompson, & Eck, 1980) have shown that surface broadband albedos of many cover types have strong diurnal variations, primarily because of the solar zenith angle dependence. The objective of this part of the experiment was to measure diurnal cycles of the several major cover types in our test site and examine whether the empirical formulae (Liang, 2001) are valid at different solar zenith angles.
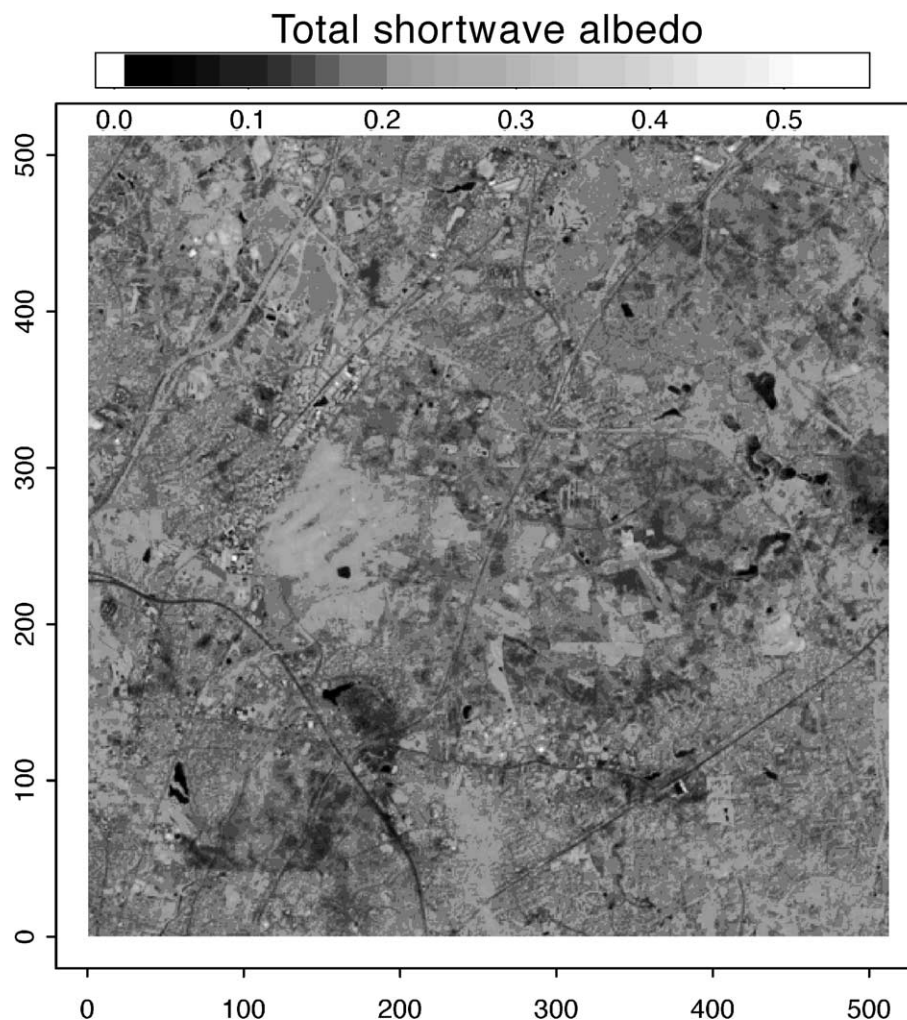

Fig. 10. Total shortwave albedo derived from ETM+ imagery of May 11, 2000 over the USDA BARC validation site at Beltsville, MD.
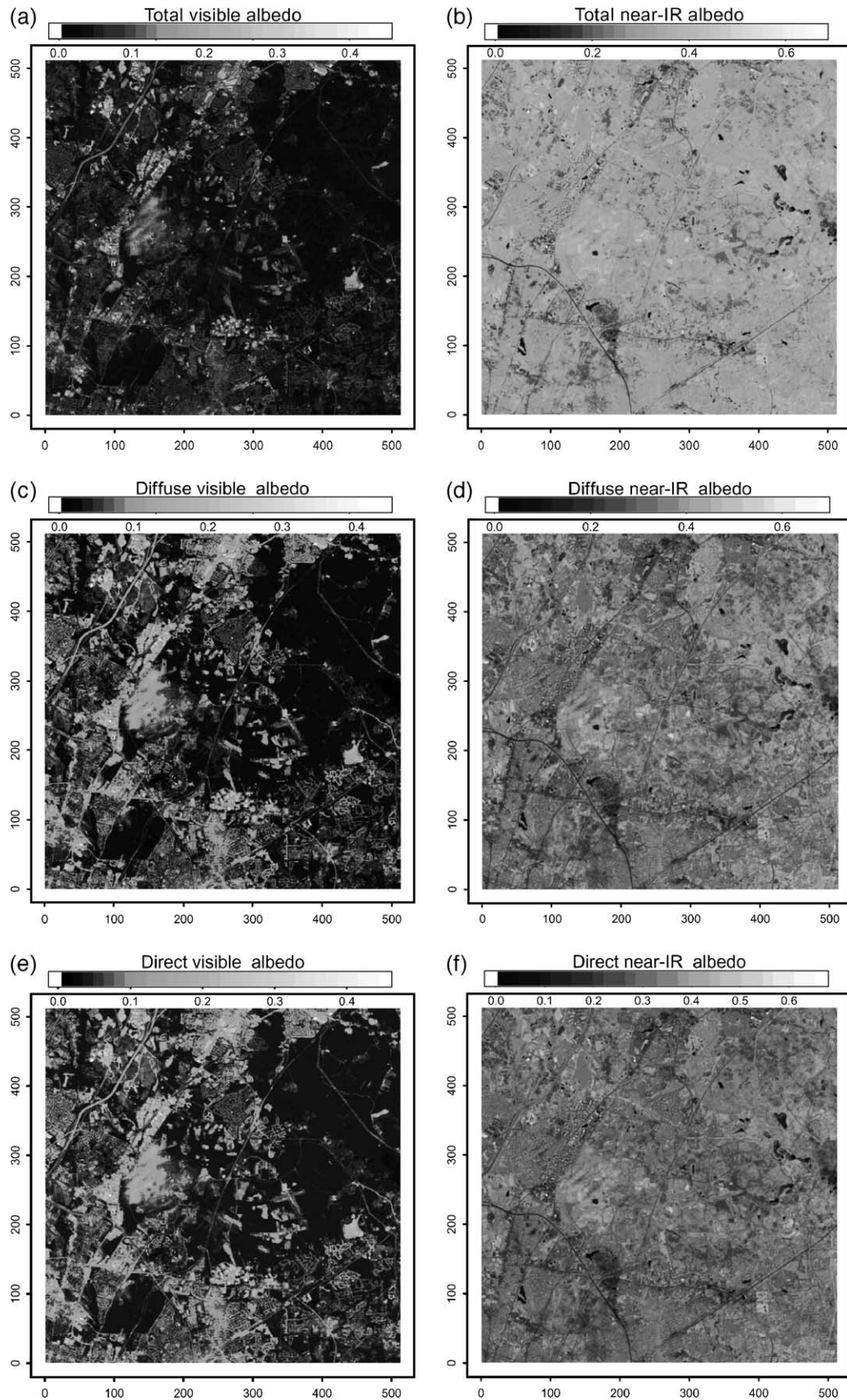
Fig. 11. Six visible and near-IR broadband albedos derived from ETM+ imagery of May 11, 2000 over the USDA BARC validation site at Beltsville, MD.

Three cover types were measured: green crop (February 26), yellow grass (March 1) and an asphalt surface (March 28), which are displayed in Fig. 2. The measured total downward flux and three albedos on three dates are shown in Fig. 3. The downward fluxes indicate the atmospheric conditions. For example, it is easy to tell the period of cloudy sky around 10–11 am on February 26 and around 3:30 pm on March 1. The cloudy albedos are different from clear-sky albedos. For green canopy, the shortwave albedo decreases from 0.23 when the sky is clear to about 0.17 when cloudy, although the total visible and near-IR albedos decrease only slightly. For dry grass, the shortwave albedo decreases from 0.21 when the sky is clear to about 0.17 when cloudy, the total near-IR albedo decreases from 0.31 to 0.25, and the total visible albedo decreases much less.

It is interesting to note the dependences of the broadband albedos on the solar zenith angles, particularly total shortwave and near-IR albedos for green vegetation and total shortwave albedo dry grass. The asphalt surface does not have much solar zenith angle dependence.

5. Validation results

After acquiring the ground measurements, data analysis is straightforward. The measured reflectance spectra were integrated with sensor spectral response functions to generate the spectral albedos (assuming Lambertian surfaces), which were then further converted using the conversion formulae developed in the previous paper (Liang, 2001). The converted broadband albedos were finally compared with the measured broadband albedos. Two indices were used to measure the goodness of fit from any standard multiple regression analysis. A multiple R^2 value indicat-

ing the correlation between the predicted and the measured broadband albedos is defined as

$$R^2 = \frac{\Sigma(\hat{Y} - \overline{Y})^2}{\Sigma(Y - \overline{Y})^2} \tag{4}$$

where $\hat{Y}$ and $\overline{Y}$ are the fitted and average broadband albedo.

Residual standard error (RSE) indicating the deviation of the points from the regression line is defined as

$$S_e = \sqrt{\frac{\Sigma(\hat{Y} - Y)^2}{n - k - 1}} \tag{5}$$

where n and k are the numbers of observations and predictors (narrow bands), respectively.

Multiple R^2 is affected by the range of albedo spanned by the data points and therefore only suitable for the comparison of different sensors for the same data sets. The second index (RSE) better indicates the uncertainty in predicting albedos. The results are presented for the individual sensors in the following text.

5.1. ASTER

The three measured and predicted broadband albedos are shown in Fig. 4. The overall R^2 exceeds 0.8 in all three bands, but the R^2 for the near-IR band exceeds 0.96. Although the residual standard errors are similar, the relative error (RSE) is smaller since near-IR albedo values are much larger. Note that we did not use all bands for predicting the total shortwave albedo.

5.2. AVHRR

Although there are only two bands, we developed a nonlinear conversion formula. The validation results are
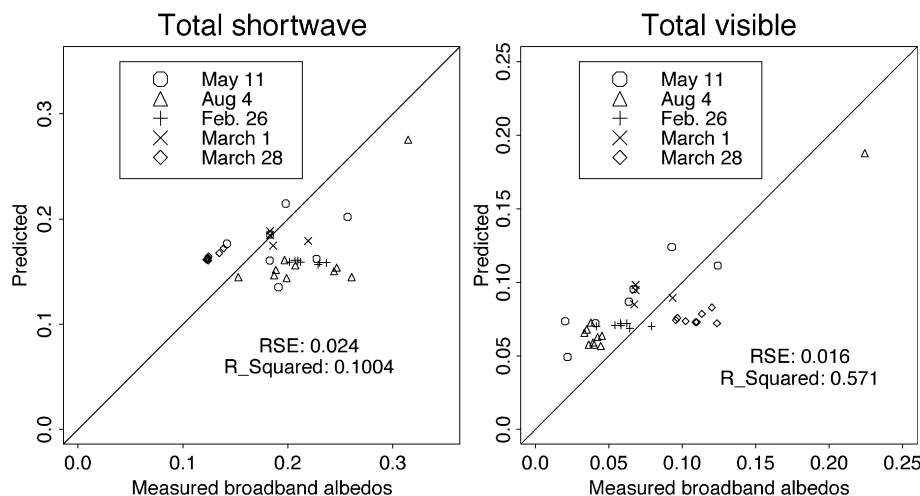

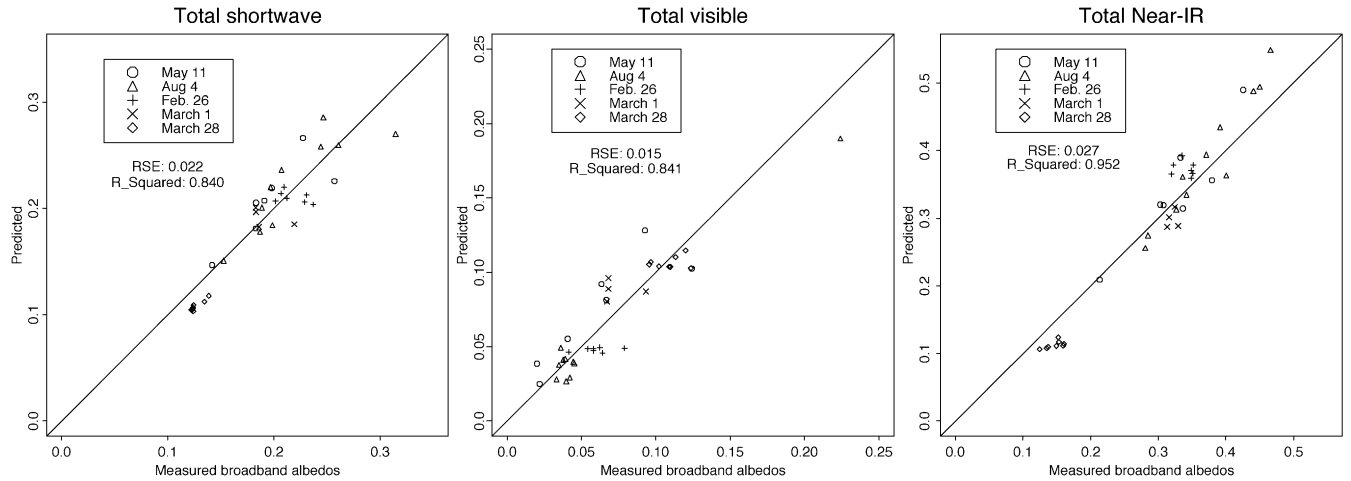Fig. 12. Comparison of the measured and predicted two broadband albedos from GOES.

Fig. 13. Comparison of the measured and predicted three broadband albedos from MISR.

shown in Fig. 5. It is surprising to find out that the R^2 values are very high, no worse than any other multispectral sensors considered in this study. It is not clear at this point if these formulae work well just for these datasets collected in our validation site. To draw a more general conclusion, further validation is needed. Nevertheless, the initial results are very encouraging.

Fig. 6 compares the predicted shortwave albedos by four representative formulae published in the literature with the ground measured data. The formula developed by Valiente et al. (1995) for vegetation/soil cover types matches with our measurements of soil/vegetation very well. Although the formula developed by Stroeve et al. (1997) was for snow, it also matches our measurements reasonably well. But the formulae by both Key (1996) and Russell et al. (1997) overestimate the total shortwave albedo. Our formula performs the best. Note again that these measurement data sets are completely independent and were not used in our formulae development.

5.3. ETM+/TM

The ETM+/TM validation results are displayed in Fig. 7. The overall correlations and residual patters are similar to ASTER.

Fig. 8 compares two formulae developed by Brest and Goward (1987) for vegetation/soil and Duguay and LeDrew (1992) with our measurement data. It is clear that the first formula overestimates and the latter underestimates, and our formula performs much better.

The Landsat7 ETM+ imagery acquired on May 11, 2000 was first corrected atmospherically using a new algorithm (Liang, Fang, & Chen, 2001). Fig. 9 shows band 4 (near-IR) images before and after atmospheric correction. Cloud still remains in the corrected imagery, but a patch of shadows has been removed. It is very clear that near-IR broadband albedo is very sensitive to cloud shadows. Assuming the surface is Lambertian, the retrieved surface spectral reflectances are numerically
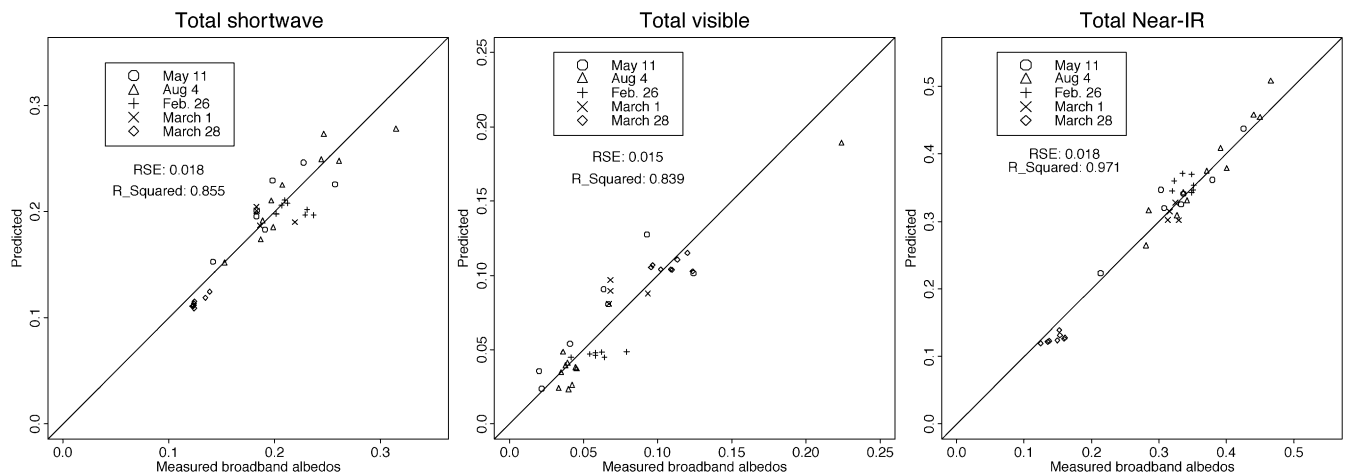

Fig. 14. Comparison of the measured and predicted three broadband albedos from MODIS.
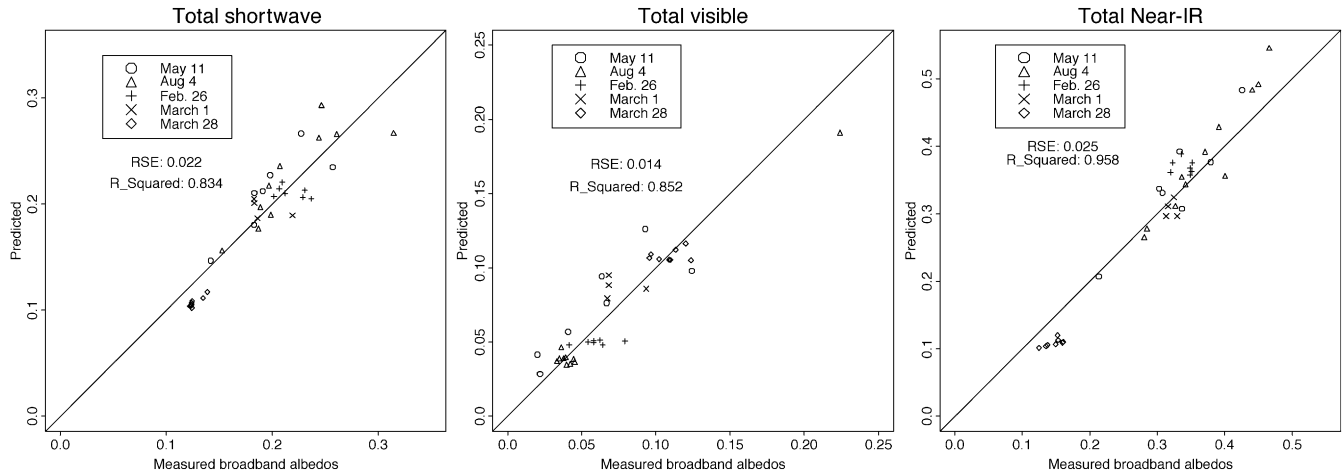
Fig. 15. Comparison of the measured and predicted three broadband albedos from POLDER.

equivalent to spectral albedos. The broadband albedos converted from these spectral albedos are shown in Figs. 10 and 11. For vegetated land, the visible albedo is small and the total shortwave and near-IR albedos are large. The direct and diffuse albedos look similar to the total albedos.

5.4. GOES

As we discussed in our previous paper (Liang, 2001), GOES has only one imaging channel and cannot predict the total shortwave albedo and near-IR albedos accurately. This is verified in our study. The validation results are shown in Fig. 12. It is obvious that GOES imager cannot predict the land surface shortwave broadband albedo reliably. Unfortunately, land surface shortwave albedos from GOES are still being produced and used in many studies.

5.5. MISR

MISR has only four bands. The model fitting uncertainty is larger than MODIS and ETM+, but the overall performance of these formulae compared to the measured broadband albedos is very good (Fig. 13). Note that MISR has multiangle observation capability, and the spectral albedos are expected to be much more accurate, which may lead to more accurate broadband albedo products.

5.6. MODIS

MODIS has similar spectral bands and the validation results (Fig. 14) are very similar to ETM+. In reality, the final MODIS product should be better than ETM+ product. This is because MODIS has off-nadir capability, which will allow us to derive spectral albedo more accurately by
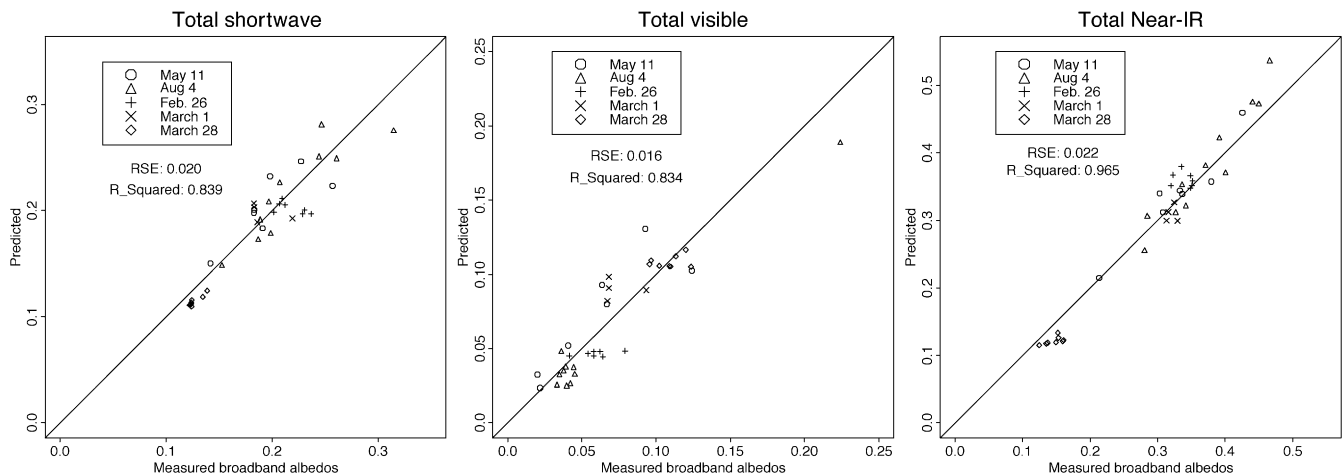

Fig. 16. Comparison of the measured and predicted three broadband albedos from VEGETATION.

considering surface BRDF effects. For ETM+, we have to assume the form of the surface BRDF.

5.7. POLDER

For POLDER the validation results (Fig. 15) are very similar to MISR. It also has simultaneous multiangle observation capability and its spectral albedo products should be more accurate than non-multiangle sensors. However, its spatial resolution is quite coarse resulting in many pixels of mixed cover types. Since these validation datasets contain several cover types, we do not anticipate poor performance for POLDER data. We are not aware of any conversion formulae in the literature for a comparison.

5.8. VEGETATION

VEGETATION is very similar to AVHRR, but it has more bands. Its conversion formulae are linear, but the validation results look very good (Fig. 16). We also are not aware of any published conversion formulae in the literature for a comparison.

6. A brief conclusion

Ground measurements have been used to validate the conversion formulae developed in the previous paper from narrowband to broadband albedos for a series of narrowband sensors. The average residual standard error (RSE) of three broadband albedos (total-shortwave, -visible, and -near-IR) is about 0.02 for most sensors. Some sensors with multispectral bands have lower errors, but GOES data (one imaging band) has much larger errors. Note that the RSE is not much larger than that in fitting these formulae, about 0.01–0.02 for total shortwave albedo, 0.002–0.2 for total visible albedo, and 0.01–0.03 for total near-IR albedo. The fitted RSE is also much smaller than the desired accuracy (about 0.05) of total shortwave by many land surface models.

The albedo differences may be attributed to several factors, over and above the limitations of the conversion formulae. In this experiment, surface reflectance spectra at nadir were collected and integrated to spectral bands. Ideally, albedo spectra should be collected. We are not familiar with any instruments on the market that perform this type of measurement. An alternative and straightforward approach is to set up a multiangle measurement scheme (Walthall, Roujean, & Morisette, 2000), and calculate the spectral albedos by angular integration of directional reflectance spectra.

Another factor is the surface heterogeneity. There is no perfect homogeneous scene at the scale of the ASD radiometer FOV. The current experiment implicitly assumes that the proportion of different covers sampled by the radiometers represents the actual proportions so that a simple average of reflectance spectra was employed. The alternative solution is to obtain proportions from images at much finer resolutions and then assign certain weights to certain cover types.

Given the statistical nature of the conversion formulae, it might be unnecessary to implement a very sophisticated field experiment. We feel confident that the average error based on data in the current experiments is a good indication of the actual error. The uncertainty of these conversion formulae for snow/ice and other surface types needs to be validated in the future.

References

Brest, C. L., & Goward, S. (1987). Deriving surface albedo measurements from narrowband satellite data. *International Journal of Remote Sensing*, *8*, 351–367.

Dickinson, R. E. (1983). Land surface processes and climate-surface albedos and energy balance. *Advances in Geophysics*, *25*, 305–353.

Duguay, C. R., & LeDrew, E. F. (1992). Estimating surface reflectance and albedo from Landsat-5 Thematic Mapper over rugged terrain. *Photogrammetric Engineering and Remote Sensing*, *58*, 551–558.

Grant, I. F., Prata, A. J., & Cechet, R. P. (2000). The impact of the diurnal variation of albedo on the remote sensing of the daily mean albedo of grassland. *Journal of Applied Meteorology*, *39*, 231–244.

Justice, C., Starr, D., Wickland, D., Privette, J., & Suttles, T. (1998). EOS land validation coordination: an update. *The Earth Observer*, *10*(3), 55–60.

Key, J. (1996). *The cloud and surface parameter retrieval (CASPR) system for polar AVHRR, Version 1.0: user's guide*. Boston University.

Kiehl, J. T., Hack, J. J., Bonan, G. B., Boville, B. A., Briegleb, B. P., Williamson, D. L., & Rasch, P. J. (1996). *Description of the NCAR Community Climate Model, NCAR Technical Note NCAR/TN-420+STR*. Boulder, CO: National Center for Atmospheric Research (152 pp.).

Kimes, D. S., Sellers, P. J., & Newcomb, W. W. (1987). Hemispherical reflectance variations of vegetation canopies and implications for global and regional energy budget studies. *Journal of Climate and Applied Meteorology*, *26*, 959–972.

Koster, R., & Suarez, M. (1992). Modeling the land surface boundary in climate models as a composite of independent vegetation stands. *Journal of Geophysical Research*, *97*, 2697–2715.

Liang, S. (2001). Narrowband to broadband conversions of land surface albedo: I. Formulae. *Remote Sensing for Environmental Sciences*, *76*, 213–238.

Liang, S., Fang, H., & Chen, M. (2001). Atmospheric correction of Landsat ETM+ land surface imagery: I. Methods. *IEEE Transactions on Geoscience and Remote Sensing*, *39*, 2490–2498.

Liang, S., Stroeve, J. C., Grant, I. F., Strahler, A. H., & Duvel, J. P. (2000). Angular corrections to satellite data for estimating earth's radiation budget. *Remote Sensing Review*, *18*, 103–136.

Morisette, J., Privette, J., Justice, C., Olson, D., Dwyer, J., Davis, P., Starr, D., & Wickland, D. (1999). The EOS land validation core sites: background information and current status. *The Earth Observer*, *11*, 11–26.

Pinker, R. T., Thompson, O. E., & Eck, T. F. (1980). The albedo of a tropical evergreen forest. *Quarterly Journal of Royal Meteorological Society*, *106*, 551–558.

Russell, M., Nunez, M., Chladil, M., Valiente, J., & Lopez-Baeza, E. (1997). Conversion of nadir, narrowband reflectance in red and near-infrared channels to hemispherical surface albedo. *Remote Sensing for Environmental Sciences*, *61*, 16–23.

Sellers, P., Randall, D. A., Collatz, G. J., Berry, J. A., Field, C. B., Dazlich, D. A., Zhang, C., Collelo, G. D., & Bounoua, L. (1996). A revised land surface parameterization (SiB2) for atmospheric GCMs. Part I. model formulation. *Journal of Climate*, *9*, 676–705.

Stroeve, J., Nolin, A., & Steffen, K. (1997). Comparison of AVHRR-derived and in-situ surface albedo over the Greenland ice sheet. *Remote Sensing and Environmental Sciences*, *62*, 262–276.

Valiente, J., Nunez, M., Lopez-Baeza, E., & Moreno, J. (1995). Narrow-band to broad-band conversion for Meteosat-visible channel and broad-band albedo using both AVHRR-1 and -2 channels. *International Journal of Remote Sensing*, *16*, 1147–1166.

Walthall, C., Roujean, J. L., & Morisette, J. (2000). Field and landscape BRDF optical wavelength measurements: experiment, techniques and the future. *Remote Sensing Review*, *18*, 503–531.